



HAL
open science

Negatively charged chitosan nanoparticles prepared by ionotropic gelation for encapsulation of positively charged proteins

Melissa Marques Gonçalves, Daniela Florencio Maluf, Roberto Pontarolo, Cyro Ketzer Saul, Eyad Almouazen, Yves Chevalier

► **To cite this version:**

Melissa Marques Gonçalves, Daniela Florencio Maluf, Roberto Pontarolo, Cyro Ketzer Saul, Eyad Almouazen, et al.. Negatively charged chitosan nanoparticles prepared by ionotropic gelation for encapsulation of positively charged proteins. *International Journal of Pharmaceutics*, 2023, 642, pp.123164. 10.1016/j.ijpharm.2023.123164 . hal-04216263

HAL Id: hal-04216263

<https://hal.science/hal-04216263>

Submitted on 24 Sep 2023

HAL is a multi-disciplinary open access archive for the deposit and dissemination of scientific research documents, whether they are published or not. The documents may come from teaching and research institutions in France or abroad, or from public or private research centers.

L'archive ouverte pluridisciplinaire **HAL**, est destinée au dépôt et à la diffusion de documents scientifiques de niveau recherche, publiés ou non, émanant des établissements d'enseignement et de recherche français ou étrangers, des laboratoires publics ou privés.

Negatively charged chitosan nanoparticles prepared by ionotropic gelation for encapsulation of positively charged proteins

Melissa Marques Gonçalves^{a,b}, Daniela Florencio Maluf^b, Roberto Pontarolo^b, Cyro Ketzer Saul^b, Eyad Almouazen^a, Yves Chevalier^a

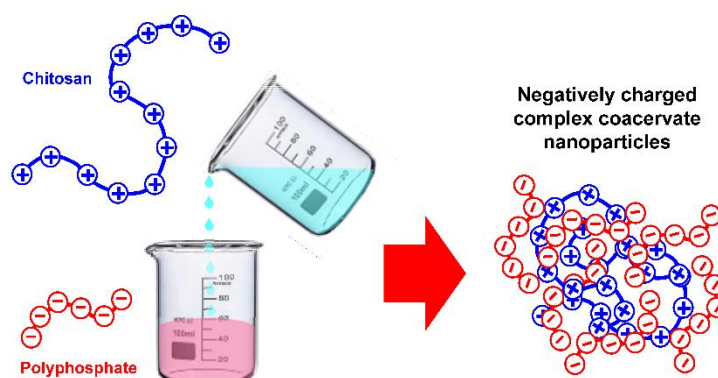
^a *Laboratory of Automatic Control, Chemical and Pharmaceutical Engineering (LAGEPP), University Claude Bernard Lyon 1, 69622 Villeurbanne, France.*

^b *Federal University of Paraná (UFPR), 80210-170, Curitiba, Brazil.*

Abstract

The nanoprecipitation of hydrogel nanoparticles by complex coacervation is investigated through a systematic study of the popular chitosan-polyphosphate pair of polyelectrolytes with opposite charges at pH 4. Polyphosphates of varying molar masses and electrical charges are investigated as alternatives to the commonly used tripolyphosphate, so as to assess the influence of the strength of electrostatic interactions on the fabrication possibility, the size of hydrogel particles, and their overall charge. Sodium hexametaphosphate and sodium polyphosphate allow the manufacture of such nanoparticles with either a positive or a negative charge, depending on the chitosan/polyphosphate ratio and the order of mixing. The classical way of mixing by pouring the polyphosphate solution into the chitosan solution yields microparticles. Inverting the order of mixing by pouring the chitosan solution into the polyphosphate solution allows the precipitation of negatively charged nanoparticles with diameters in the range 100–200 nm. Such charge inversion of the chitosan into negative is not possible with the common TPP. It was achieved using sodium hexametaphosphate and sodium polyphosphate having a larger negative charge. Charge inversion of chitosan allows an efficient encapsulation of positively charged proteins with an improved encapsulation efficiency than in the usual TPP-based coacervate. The encapsulation of the bovine serum albumin at pH 4 is given as a case study of a positively charged protein.

Keywords: Complex coacervation, nanoparticles, chitosan, polyphosphate, hexametaphosphate, tripolyphosphate, phytic acid



1. Introduction

Encapsulation inside polymer particles is a way to protect active pharmaceutical ingredients (API) against their degradation and/or to control their release. Hydrophilic API like proteins are usually encapsulated in porous polymer particles prepared from double emulsions or hydrogel particles made of cross-linked water-soluble polymers. Biocompatible and biodegradable polymers are used to this end. Chitosan is a carbohydrate polymer that presents such characteristics. In addition, chitosan itself shows interesting properties in the framework of drug delivery such as antimicrobial and mucoadhesive activities. Particles of cross-linked chitosan are most often prepared by either chemical cross-linking inside the water droplets of a w/o emulsion or by coacervation methods. Coacervation is preferred because of its simpler implementation and the absence of organic solvents that elimination may be difficult. Chemical cross-linking involves harmful reagents that also may react with the active substances. Both these features are important for going to practical applications [1–6].

Ionotropic gelation is a very efficient type of coacervation allowing the preparation of chitosan particles. It involves electrostatic interactions between positively charged primary amino groups of chitosan and negatively charged polyanions acting as cross-linking agents. This physical process is reversible, which prevents not only the toxicity to the organism, but also the drugs damage [7–9].

Many of the medical and pharmaceutical applications of chitosan rely on its positive charge. The use of chitosan nano- and microparticles in gene therapy is an example since the negatively charged genetic materials electrostatically bind with the chitosan, allowing their encapsulation. However, the encapsulation efficiency of positively charged materials in these particles is low because electrostatic repulsions prevent binding. This is the case of the widely studied bovine serum albumin (BSA) at pH below its isoelectric point where it is positively charged [10]. Positively charged materials strongly interact with serum components, causing their rapid clearance from circulation after parenteral administration [11]. It is useful to encapsulate them into negatively charged (nano)particles in order to remedy this issue. To overcome these limitations, chemical modifications of chitosan or particles coating are frequently used [12–17]. The present paper reports a simpler method by complex coacervation.

So far, stable negatively charged chitosan/polyanion particles were not reported in the literature. We are presenting an unprecedented way of obtaining negatively charged nano- and microparticles of chitosan/polyanions that allows increasing the encapsulation efficiency of positively charged proteins. Such mild method relying on simple mixing prevents any structural alteration of chitosan and avoids the implementation of an extra step of particle coating or chemical modification. This is achieved by a modification of the classic ionotropic gelation technique.

The most popular ionotropic gelation system is made of mixed chitosan/tripolyphosphate (Ch/TPP) [1–7,9,14–16,18–28]. Owing to the high dissymmetry of molar masses and electrical charges of chitosan and TPP, the charge of hydrogel nanoparticles is set by the polyelectrolyte of highest molar mass and charge, namely the positively charged chitosan. It is hypothesized that increasing the molar mass and charge of the polyphosphate counterpart may allow the manufacture of both positively and negatively charged hydrogel nanoparticles, thereby opening possible encapsulation of proteins of both charges with high encapsulation efficiency. Therefore, the complex coacervation of chitosan with several polyphosphates was investigated with the aim of reversing the charge of chitosan during nanoparticles precipitation. The

polyphosphates having different numbers of phosphate groups and negative charges were orthophosphate (P), pyrophosphate (Py), tripolyphosphate (TPP), hexametaphosphate, (HMP) polyphosphate (PP) and phytic acid (PA) (Figure 1).

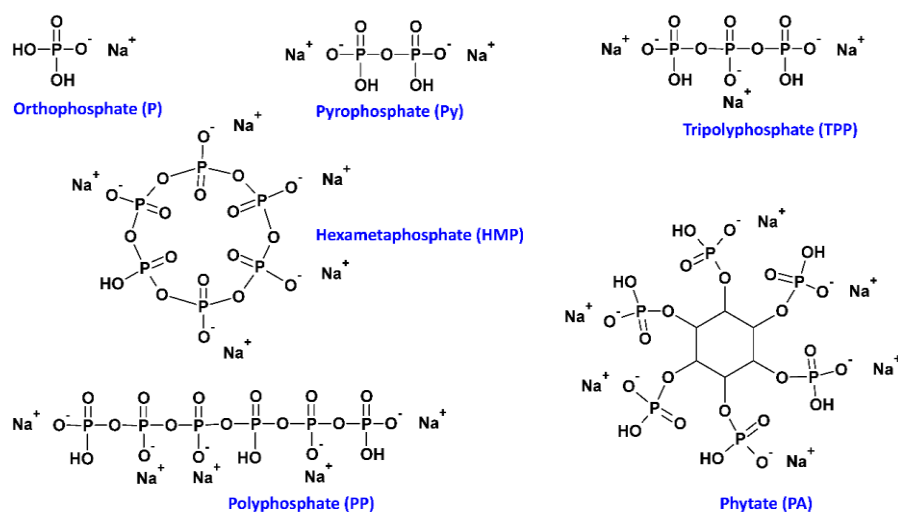


Figure 1. Chemical structure of the six polyphosphates studied for the complex coacervation with chitosan. The polymerization degree of the compound named “polyphosphate” is not known; it is given here with an arbitrary value of 6. The given ionic form of the polyphosphates is that pertaining to pH 4 at which coacervation experiments were performed.

2. Material and Methods

2.1. Materials

Chitosan (Ch) of low-viscosity grade from shrimp shells (CAS 9012-76-4) was purchased from Sigma-Aldrich. Its degree of acetylation was $DA = 20\%$ as determined from its ^1H NMR spectrum in $\text{D}_2\text{O}/\text{DCl}$ solution given in the [Supplementary Material](#) file [29–31]. Its number-average and mass-average molar masses determined by SEC analysis were $M_N = 9.95 \cdot 10^4 \text{ g}\cdot\text{mol}^{-1}$ and $M_W = 2.60 \cdot 10^5 \text{ g}\cdot\text{mol}^{-1}$ (see the [Supplementary Material](#) file). Di-sodium hydrogen orthophosphate dodecahydrate (CAS 7558-79-4), sodium pyrophosphate tetrabasic decahydrate (CAS 13472-36-1), sodium triphosphate pentabasic (CAS 7758-29-4), sodium hexametaphosphate (CAS 68915-31-1), sodium polyphosphate (CAS 10361-03-2), phytic acid sodium salt hydrate (CAS 14306-25-3) were purchased from Sigma-Aldrich. Their chemical analyses by ^{31}P NMR in 1 M HEPES buffer at pH 5.5 and by MP-AES are reported in the [Supplementary Material](#) file. Bovine serum albumin (BSA, CAS 9048-46-8) and Bradford dye reagent (CAS 7664-38-2) were purchased from Thermo Fisher Scientific. Analytical grade chemicals and ultrapure water of $18 \text{ M}\Omega\cdot\text{cm}$ resistivity were used in all experiments.

2.2. Preparation of chitosan/polyphosphate complex coacervate particles

All preparations were done at the room temperature regulated at 20°C . Chitosan nano- and microparticles were obtained using a modified ionic gelation technique [18,19]. Sodium pyrophosphate tetrabasic decahydrate, sodium triphosphate pentabasic, sodium polyphosphate, sodium hexametaphosphate and phytic acid sodium salt hydrate were used as anions. Several masses: 20 mg, 30 mg, 40 mg, 50 mg, 100 mg and 500 mg were dissolved in 20 mL of water and their pH was adjusted at 4 by addition of sodium hydroxide. A $1 \text{ g}\cdot\text{L}^{-1}$ aqueous solution of chitosan at pH 4 was prepared; the pH was adjusted by addition of acetic acid. All the

polyphosphate solutions (20 mL at pH 4) were mixed with 50 mL of chitosan solution by either pouring the anionic polyphosphate solution into the cationic chitosan solution or the cationic chitosan solution into the anionic polyphosphate solution. The solutions were added into the other solution stirred with a magnetic bar at a speed of 500 rpm using a 50 mL glass syringe of 2 mm opening diameter setting a flow rate of $3 \text{ mL}\cdot\text{s}^{-1}$. The samples immediately turned cloudy as mixing was operating.

2.3. Preparation of BSA-loaded particles

BSA-loaded particles were prepared using two formulations selected out of the 60 assays listed in section 2.2. 1 mg of BSA was added to the chitosan solution (5 mg in 5 mL of ultrapure water at pH 4) and mixed into the polyanion solution (10 mg in 2 mL of ultrapure water at pH 4) in the same way as for the preparation of blank particles.

2.4. Characterization of chitosan nano- and microparticles

2.4.1. Turbidity, zeta potential (ζ) and particle size measurements

The turbidity of suspensions was measured using a Mettler-Toledo UV5 UV-vis spectrophotometer. The absorbance Abs measured in quartz cells of $l = 1 \text{ cm}$ optical path was converted into the turbidity $\tau = \ln(10) Abs/l$. Electrophoretic mobility of all formulations in 10 mM NaCl was determined using a Zetasizer Nano ZS instrument (Malvern Panalytical). The samples were contained in DTS1070 U-shaped cuvettes equipped with electrodes. The ζ potential was calculated using the Smoluchowski equation. Size distribution of nanoparticles was measured by dynamic light scattering (DLS) using a Zetasizer Nano ZS instrument (Malvern Panalytical). The suspensions were diluted with water by a factor of 10, such that the measurements did not depend on the dilution factor. The size distribution given by the CONTIN analysis of the autocorrelation function showed a single population of sizes in cases where the mean diameter was smaller than $1 \mu\text{m}$. In such cases, the z -average diameter was calculated from the experimental autocorrelation function by the method of cumulants. In cases of larger particle sizes, size measurements were performed by low-angle laser light scattering (LALLS) using a Mastersizer 3000 instrument (Malvern Panalytical). The samples were diluted in the circulating loop of the instrument such that the obscuration reached values between 2% and 5%. The refractive index of the particles was close to that of water because of their extensive swelling, so that the measured size distribution did not depend on the exact value of the refractive index. It has been checked that this approximation was valid by performing a series of measurements where the refractive index of particles was varying from 1.335 to 1.37. A refractive index of 1.35 was taken in all measurements. All measurements were performed in triplicate by three different samplings taken in the same batch, and the error bars were the *sem* calculated from the three mean sizes.

2.4.2. Transmission electron microscopy (TEM)

TEM observations were done at the “Centre Technologique des Microstructures” of the University of Lyon 1 (CTμ, <http://microscopies.univ-lyon1.fr/>) using a Jeol 1400 Flash electron microscope. The aqueous suspensions were diluted by 1/100 and a drop of $5 \mu\text{L}$ was deposited on a formvar/carbon grid for drying. TEM observations were done under 120 kV acceleration at several magnifications.

2.4.3. Determination of the Encapsulation Efficiency of BSA

The encapsulation efficiency (*EE*) of BSA was determined by measurements of the amounts of encapsulated and free BSA by the Bradford method. The samples were centrifuged at 170000 g RCF for 1 h at 4 °C with an ultracentrifuge Optima MAX-XP (Beckman Coulter). The sediment was redispersed into 100 times its volume of water for its analysis. Both the supernatant and redispersed sediment were mixed with the Bradford reagent and their absorbance was measured at 595 nm wavelength in quartz cuvettes of 10 mm optical path with a spectrophotometer UV5 (Mettler Toledo). BSA concentrations were calculated from the calibration curve of absorbance (*Abs*) determined for concentrations up to 16 mg·L⁻¹ and regressed to a 3rd degree polynomial as $C \text{ (mg}\cdot\text{L}^{-1}) = 106.5 Abs^3 - 16.2 Abs^2 + 6.9 Abs + 0.1$ (Figure S5 in the Supplementary Material file). The *EE* was calculated as the ratio of the BSA mass in the sediment to the total mass. It has been successfully checked that the total balance matched the full BSA amount, showing that there was no significant loss or degradation of BSA during the processes.

3. Results and Discussion

3.1. Description of polyphosphates at pH 4

The usual process of complex coacervation of chitosan with TPP consists in mixing them by pouring the TPP solution into the chitosan solution [20]. The amount of TPP is restricted below the charge stoichiometry of the mixture. Because a low amount of TPP is added, TPP is referred to as a cross-linking agent. Under such conditions of excess positive charge coming from the chitosan, only positively charged particles can be obtained. It may be expected that addition of more TPP would invert the charge into negative. However, when the particle charge passes through zero at exact charge compensation, the neutral particles aggregate because of their loss of electrostatic stabilization. Consequently, very large lumps of aggregates are recovered at the end of the process. Mixing by pouring the chitosan solution into the polyphosphate solution was studied as an alternative to remedy this trouble. The two ways of mixing were presently studied in a systematic investigation where the hydrogel nanoprecipitation, the particle size and zeta potential were monitored after mixing 50 mL of chitosan solution (1 g·L⁻¹) and 20 mL of polyphosphates solutions of various concentrations in the range 1 – 25 g·L⁻¹. After mixing, the concentration of chitosan was 0.71 g·L⁻¹ in all samples; and the range of polyphosphate concentrations was 0.28 – 7.14 g·L⁻¹. Polyphosphates of higher charge than TPP were investigated in order to reduce the charge dissymmetry of the pair of polyelectrolytes and closer approach the standard precipitation process by complex coacervation of mixed polyelectrolytes.

The six studied polyphosphates are given as follows in order of increasing charge set by their number of phosphate groups: $n = 1$ for orthophosphate (P), $n = 2$ for pyrophosphate (Py), $n = 3$ for tripolyphosphate (TPP), $n = 6$ for hexametaphosphate (HMP) and phytate (PA), and $n \approx 6$ as average value for polyphosphate (PP) (Table 1). In all experiments, the pH was set at 4 by addition of glacial acetic acid for chitosan was soluble in water. The electrical charge of polyphosphates at pH 4 might be calculated from their pK_A 's. Unfortunately, most of them are not documented. Their electrical charge at pH 4 was determined from their chemical analysis and the volume of acid required to set pH = 4; and they were also calculated from their pK_A values when their values were available (see the Supplementary Material file).

Table 1. List of the studied polyphosphates together with their number of phosphorus atoms and negative electrical charge at pH 4.

Type of sodium polyphosphate	Number of phosphorus atoms	Charge at pH 4 from titration	Charge at pH 4 calculated from pK_A 's
Orthophosphate (P)	$n = 1$	-0.97	-0.99
Pyrophosphate (Py)	$n = 2$	-1.94	-1.99
Triphosphate (TPP)	$n = 3$	-3.03	-2.98
Hexametaphosphate (HMP)	$n = 6$	-5.0	–
Polyphosphate (PP)	$n \approx 6$	-5.0	–
Phytate (PA)	$n = 6$	-6.04	-6.01

3.2. Precipitation by complex coacervation

Complex coacervation of chitosan was not possible with sodium orthophosphate at pH 4. This was quite an expected result because the charge of sodium orthophosphate is -1 under its dihydrogen phosphate form NaH_2PO_4 . Any binding of this monovalent anion to chitosan only results in a simple monovalent anion exchange of dihydrogen phosphate for acetate. This cannot cause electrostatic cross-linking. Complex coacervation was observed with all other polyphosphates of higher negative charge, whatever the way the chitosan and polyphosphate were mixed. Samples turned cloudy very fast upon mixing because of the precipitation of particles of complex coacervate. In some cases, the samples remained homogeneous, indicating that particles were small enough for neither sedimentation nor creaming occurred. Alternatively, large lumps of coacervate settled in the liquid medium. The order of mixing chitosan and polyphosphates had a strong influence on the particle size, especially in the cases of PP and HMP. This was clearly revealed by the low turbidity of suspensions prepared by pouring Ch into PP (or HMP), contrasting with the strong cloudy aspect obtained when pouring PP (or HMP) into Ch (Figure 2). These observations were suggesting the formation of smaller particles upon pouring Ch into polyphosphate. Sedimentation took place within a few hours for samples where PP (or HMP) was poured into Ch. Gentle hand shaking easily redispersed the sediment. On the contrary, sedimentation did not occur when Ch was poured into PP (or HMP). The visual aspect stayed the same for long times, showing the colloidal stability of the suspensions.

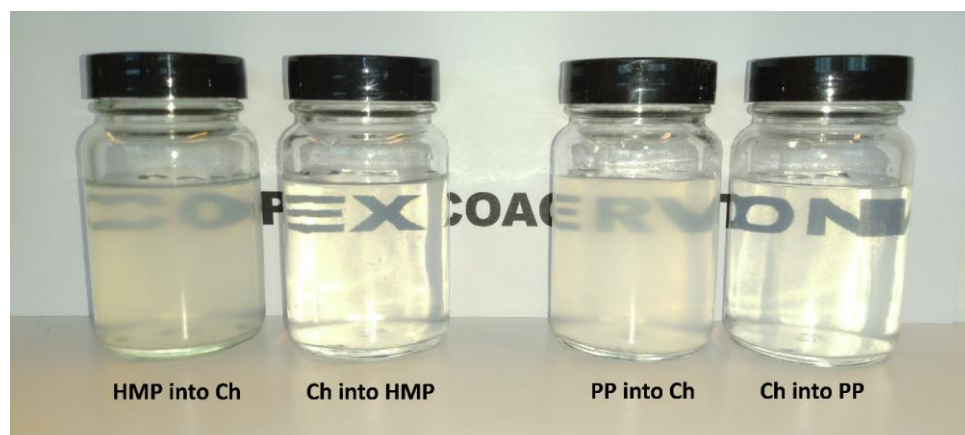


Figure 2. Aqueous suspensions of coacervate particles of chitosan ($0.714 \text{ g}\cdot\text{L}^{-1}$) and excess of HMP or PP ($1.4 \text{ g}\cdot\text{L}^{-1}$) obtained by mixing either polyphosphates into Ch or Ch into polyphosphates.

The visual observations were confirmed by turbidity measurements showing a much higher turbidity when HMP (or PP) was poured into chitosan (Figure 3). For instance, the turbidity at 600 nm wavelength was about 3–4 times larger for HMP (or PP) poured into Ch ($\tau = 0.538 \text{ cm}^{-1}$ for HMP and $\tau = 0.471 \text{ cm}^{-1}$ for PP) than for the reverse mixing order ($\tau = 0.193 \text{ cm}^{-1}$ for HMP and $\tau = 0.122 \text{ cm}^{-1}$ for PP).

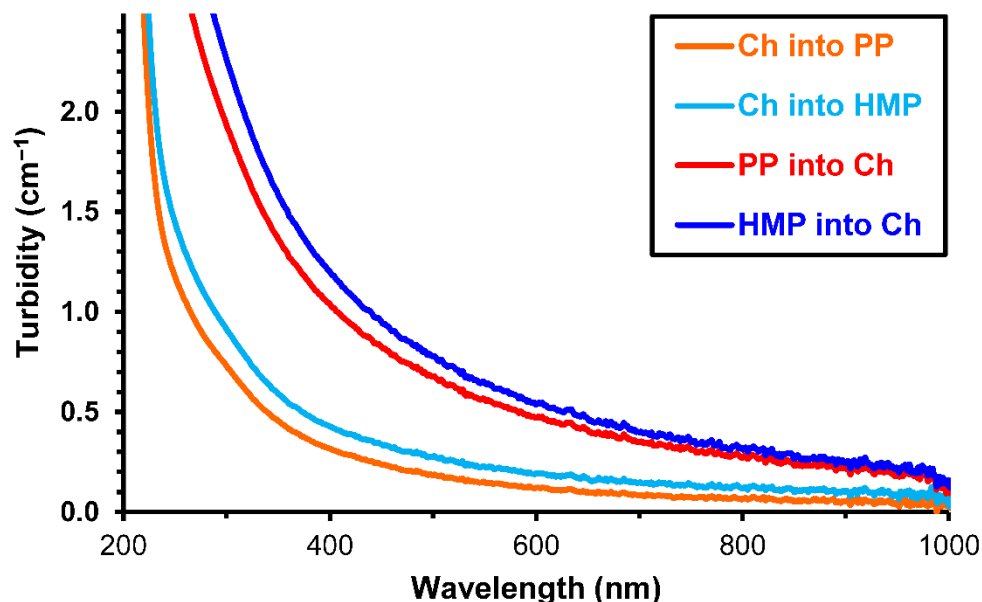


Figure 3. Turbidity of aqueous suspensions of coacervate particles of chitosan ($0.714 \text{ g}\cdot\text{L}^{-1}$) and excess of HMP or PP ($1.4 \text{ g}\cdot\text{L}^{-1}$) obtained by mixing either polyphosphates into Ch or Ch into polyphosphates.

The mean particle sizes and ζ potentials obtained for all formulations are shown in Figures 4–8. As expected, all ζ potentials decreased upon addition of polyphosphates. One exception is Ch/Py at low Py concentration. The ζ potentials of all mixed Ch/polyphosphates suspensions did not depend of the way the two components have been mixed. Such overall feature of the data suggests that the chemical composition of the particles was the same, whatever the mixing process. This may appear surprising because the compositional paths followed by mixing either polyphosphates into Ch or Ch into polyphosphates are different. The composition is rich in Ch at the beginning of pouring polyphosphates into Ch. At the opposite, it is rich in polyphosphates upon reversing the order of mixing. The final overall compositions of the coacervate particles were the same at the end of mixing. It seems that the chemical composition of the particles turned homogeneous during the course of the mixing process, although they were very different at the beginning. In the framework of the nucleation and growth mechanism of precipitation, particles of different compositions have been nucleated and their subsequent growth homogenized their composition.

Conversely, the size of the precipitated particles did change according to the way of mixing in some instances. Such dependence of particle size showed that irreversible phenomena of different natures occurred during the two mixing processes.

All particles obtained with Ch/Py had sizes in the colloidal range (less than $1 \mu\text{m}$) and presented positive zeta potential values between $9 \pm 1 \text{ mV}$ and $28.4 \pm 0.4 \text{ mV}$. The same size distribution and zeta potential patterns were observed for both mixing orders (Figure 4). The charge did not reverse to negative values, though the theoretical charge stoichiometry of Ch

was reached at a Py concentration of $1.2 \text{ g}\cdot\text{L}^{-1}$. This meant that only part of the Py bound to Ch. The increase of ζ potential with respect to low Py concentration (Figure 4) is counter-intuitive. Only these particular samples showed such paradoxical behavior. The size of nanoparticles decreased with respect to the Py concentration. Indeed, a higher Py concentration causes a faster nucleation of particles, yielding a smaller size at the end of the mixing process.

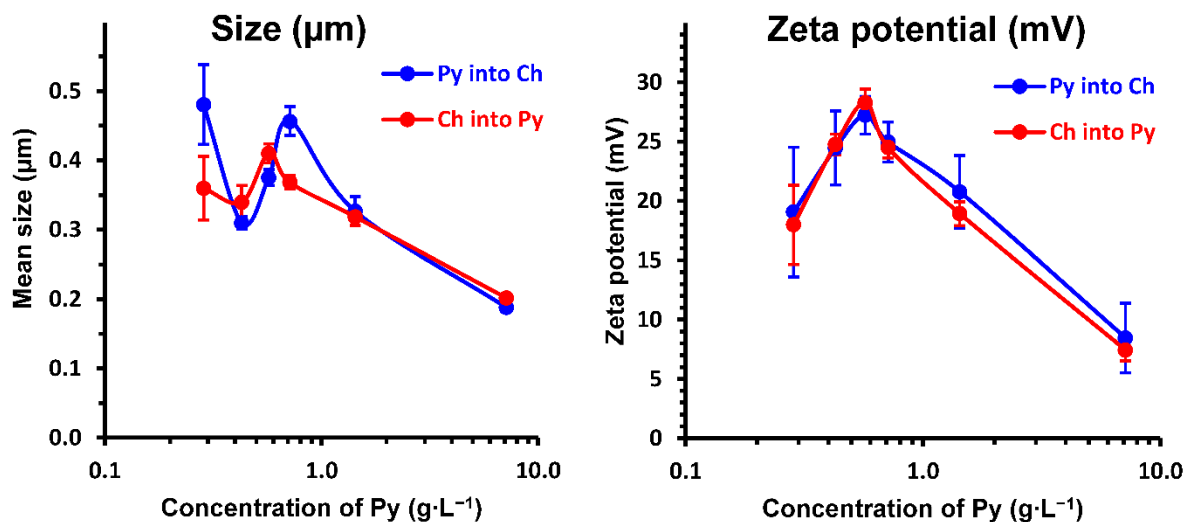


Figure 4. Behavior of mixed chitosan (Ch) and pyrophosphate (Py). z -average hydrodynamic diameter measured by DLS and ζ potential for particles obtained by mixing Py into Ch (blue) and Ch into Py (red).

Similarly, Ch/TPP particles showed the same behavior for both mixing orders (Figure 5), and only positive values of ζ potential between $3.5 \pm 0.3 \text{ mV}$ and $20.3 \pm 1.4 \text{ mV}$ were measured. These values of ζ potential were in accordance with the literature reports [27]. Stable Ch/TPP particles of negative charge could not be obtained. The lowest value of ζ potential reported in the literature was for Ch/TPP particles precipitated from a mixture of 1/8 mass ratio [25]; the slightly negative value of the ζ potential ($-2.10 \pm 7.45 \text{ mV}$) was not significantly different of zero. Negatively charged Ch/TPP particles reported in the literature could only be obtained after subsequent coating with a supplementary layer of negative polyelectrolyte such as pectin [32], alginate [33], or poly(acrylic acid) [11]. The present particles were of large sizes (average diameters between 60 and 80 μm), much higher than those reported in the literature for particles of the same composition [3,16]. As for Py, the lack of charge reversal upon passing the theoretical charge stoichiometry ($0.75 \text{ g}\cdot\text{L}^{-1}$) showed that only part of TPP bound to Ch during the coacervation and precipitation. Reinforced binding of polyanions to Ch could be achieved by Motiei *et al.* [34] upon associating TPP and dextran sulfate that is a negatively charged polyelectrolyte of high molar mass. Small nanoparticles were obtained at low TPP concentration (Figure 5). At variance with the behavior of Py, very large particles were formed at TPP concentrations larger than $0.4 \text{ g}\cdot\text{L}^{-1}$. As TPP concentration was increased, the charge of particles was lower and the residual TPP concentration in the aqueous phase increased. Both phenomena caused weakening of electrostatic repulsions between particles and their destabilization. The large size of particles resulted from the flocculation of small nanoparticles because of their poor electrostatic stabilization.

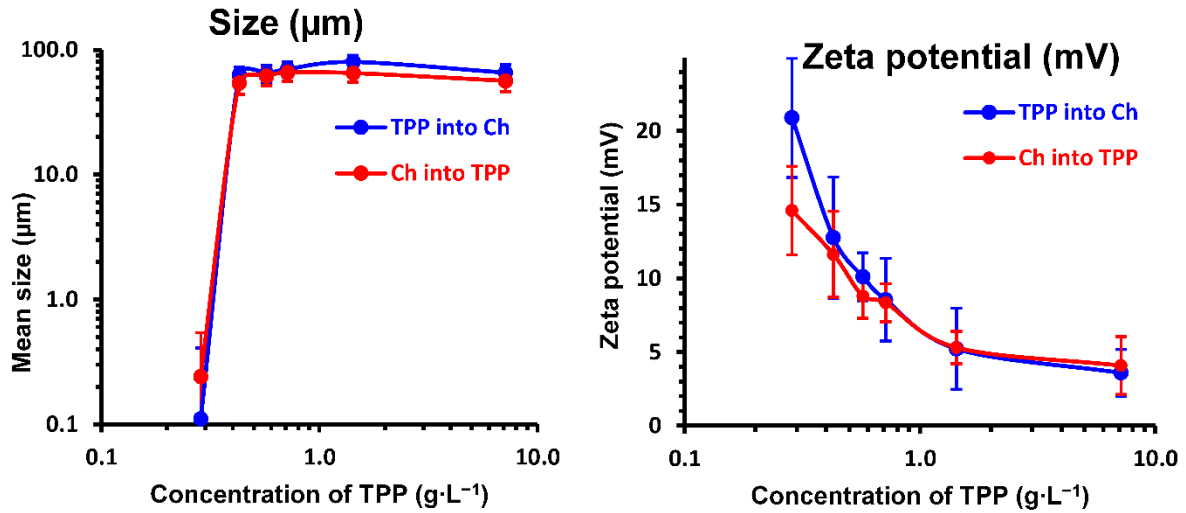


Figure 5. Behavior of mixed chitosan (Ch) and tripolyphosphate (TPP). z -average hydrodynamic diameter measured by DLS and ζ potential for particles obtained by mixing TPP into Ch (blue) and Ch into TPP (red).

The behavior of hexametaphosphate and polyphosphate (Figures 6 and 7) was quite different of the two previous ones. Indeed, the ζ potential turned from positive to negative values as the concentrations of HMP or PP were increased. Such charge reversal occurred at a concentration of HMP or PP of $0.40 \text{ g}\cdot\text{L}^{-1}$ that corresponded to a concentration of negative charge $C^- = 3.9 \cdot 10^{-3} \text{ mol}\cdot\text{L}^{-1}$ for HMP and $C^- = 3.8 \cdot 10^{-3} \text{ mol}\cdot\text{L}^{-1}$ for PP. Owing to the mass concentration of chitosan $[\text{Ch}] = 0.714 \text{ g}\cdot\text{L}^{-1}$, its acetylation degree $DA = 20\%$, and the average molar mass of the Ch repeat unit $M_{\text{mol}} = 169.57 \text{ g}\cdot\text{mol}^{-1}$, the concentration of positive charges coming from Ch is

$$C_+ = \frac{(1-DA) \times [\text{Ch}]}{M_{\text{mol}}} = \frac{0.8 \times 0.714}{169.57} = 3.37 \cdot 10^{-3} \text{ mol}\cdot\text{L}^{-1}$$

The concentrations C_+ and C^- were close each other, which indicated that the full HMP or PP bound to Ch and caused precipitation of the complex coacervate. Charge reversal occurred whatever the way of mixing. Stable nanoparticles with ζ potential values of $-23.7 \pm 1 \text{ mV}$ for HMP and $-29.4 \pm 2 \text{ mV}$ for PP were obtained. Sang *et al.* [3] investigated the precipitation by complex coacervation (that they called "cross-linking") of chitosan by mixing with several types of polyphosphates. They restricted their study to mixing by pouring polyphosphates solutions into the Ch solution and amounts of polyphosphates were below the charge stoichiometry in all cases, so that they did not report any negative ζ potential values, even for the Ch/HMP particles. Situ *et al.* [2] reported negative ζ potentials with TPP (but not with HMP). The degree of acetylation of their chitosan was not mentioned, so that this is difficult to figure out the reason why their results were different of ours. Assuming that their acetylation degree was the same as ours ($DA = 20\%$), their amounts of TPP were below the charge stoichiometry. Their experimental results are at variance with ours, and they are quite surprising owing to the TPP/Ch stoichiometry lower than charge balance. The pH in their experiments was varying up to pH 7 where Ch is of very low solubility [35].

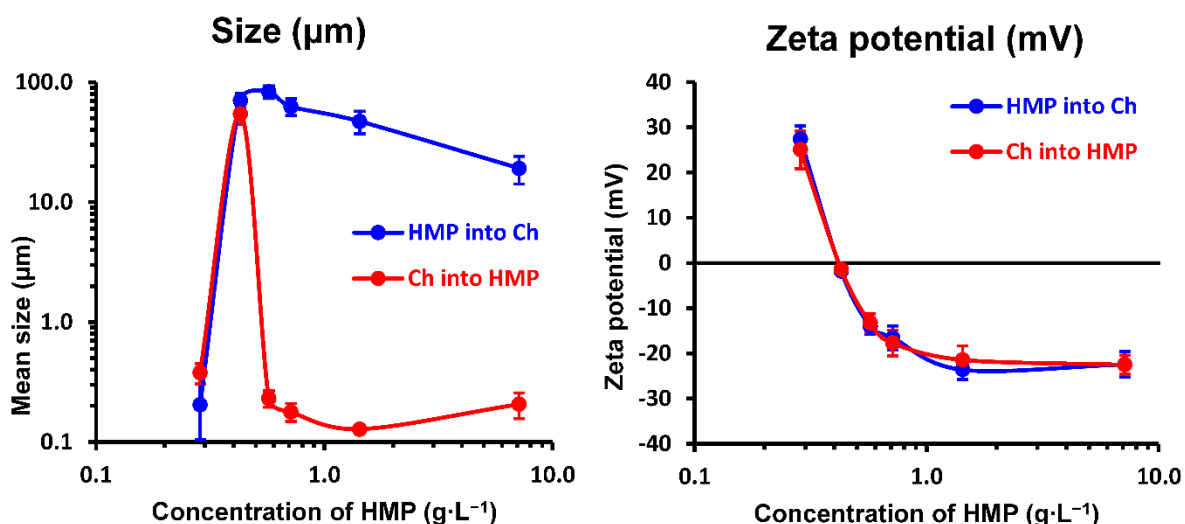


Figure 6. Behavior of mixed chitosan (Ch) and hexametaphosphate (HMP). z -average hydrodynamic diameter measured by DLS and ζ potential for particles obtained by pouring HMP into Ch (blue) and Ch into HMP (red).

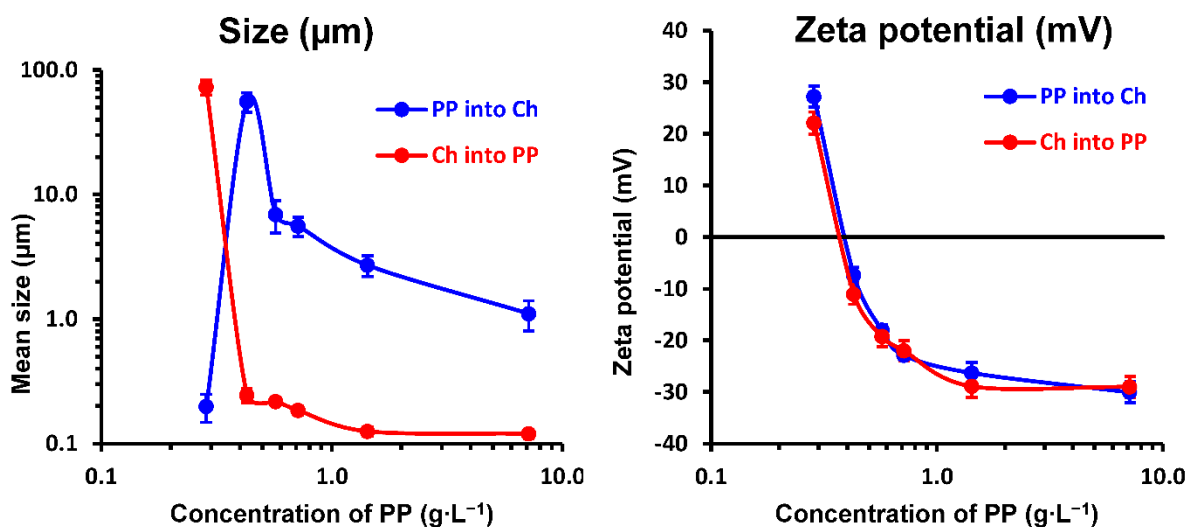


Figure 7. Behavior of mixed chitosan (Ch) and polyphosphate (PP). z -average hydrodynamic diameter measured by DLS and ζ potential for particles obtained by pouring PP into Ch (blue) and Ch into PP (red).

Another prominent feature was the different size of particles depending on the way of mixing. Microparticles with sizes in the order of 20 to 80 μm were obtained upon pouring HMP solution into Ch solution, whereas nanoparticles of approximately 120 nm were obtained by pouring Ch into HMP (Figure 6). The same trends were also observed in the case of Ch/PP precipitation (Figure 7).

These results may be due to the fact that there is no charge inversion when the positive Ch was added into the solution of negative HMP or PP and the addition was stopped before the concentration of charge reversal was reached. On the contrary, addition of the negative HMP or PP into the positive Ch so as to reach a final negative charge of the polyelectrolyte association necessarily caused a charge reversal by crossing through a transitory state of zero charge where the suspension of particles was not stable. Coagulation and coalescence caused the irreversible formation of large microparticles.

Charge reversal was also possible with phytate that had the same molecular charge as HMP and PP (Figure 8). It occurred around a PA concentration of $0.6 \text{ g}\cdot\text{L}^{-1}$, which was higher than the theoretical charge stoichiometry ($0.445 \text{ g}\cdot\text{L}^{-1}$). Large microparticles of $300 \mu\text{m}$ diameter precipitated upon pouring PA solution into Ch, excepted at low concentrations of PA (nanoparticles of 150 nm diameter were formed). Changing the mixing order also resulted in the precipitation of large microparticles of size in the range $60 - 170 \mu\text{m}$ (Figure 8).

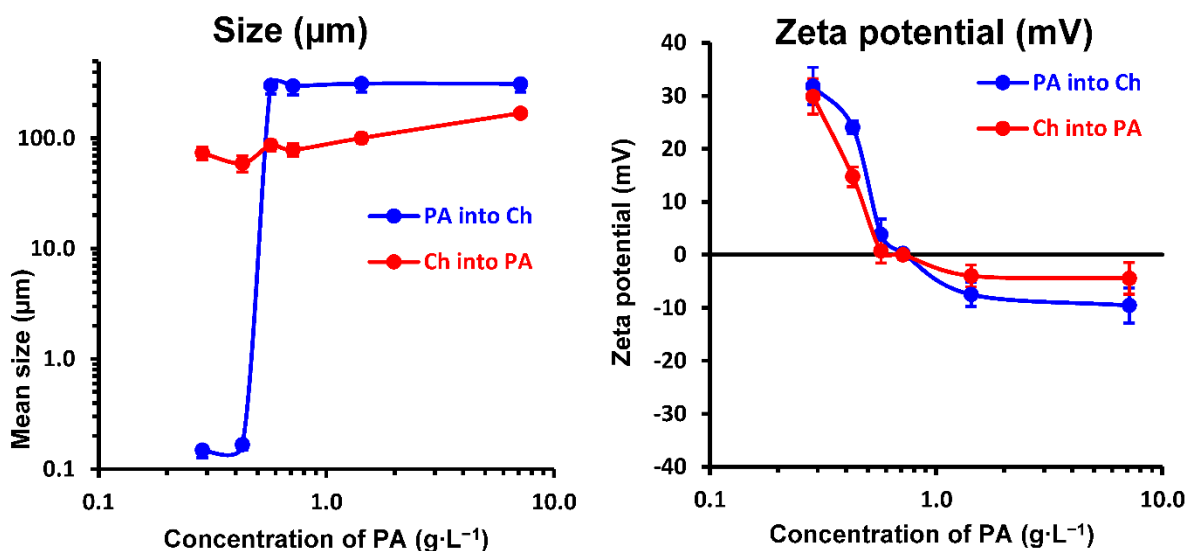


Figure 8. Behavior of mixed chitosan (Ch) and phytate (PA). z-average hydrodynamic diameter measured by DLS and ζ potential for particles obtained by pouring PA into Ch (blue) and Ch into PA (red).

As a whole, charge reversal could be achieved by pouring Ch into the polyphosphate solution when the charge of polyphosphates was at least -5 . The smallest polyphosphates of the series failed at reversing the charge of Ch because they had low negative charges of -1 (P), -2 (Py) and -3 (TPP). HMP and PP of charge -5 allowed successful charge reversal of Ch. Negatively charged nanoparticles could be precipitated by pouring a Ch solution into HMP or PP solution.

The large differences of particle size depending of the order of mixing were confirmed by TEM observations made for HMP/Ch and PP/Ch coacervate particles precipitated with an excess of HMP (or PP) with respect to the charge stoichiometry and according to the two mixing orders. The suspensions were diluted with pure water by $1/100$ and a drop of $5 \mu\text{L}$ was dried on the TEM grid. Drying the samples during the sampling process caused aggregation of a part of the particles. Indeed, the pictures showed free particles together with aggregates of them. It is not possible to know whether aggregates were already present in the suspension or were formed during drying. The small sizes measured by DLS indicated that there was no aggregation in the suspensions. The pictures showed particles that underwent degradation under the electron beam. This phenomenon described in the [Supplementary Material](#) file (Figure S6) induced a bias in observations when the samples were left under the beam for the rather long time required for adjusting the focus of the images. Fast focusing the images allowed the observation of particles with minor degradation.

The pictures of particles precipitated by pouring Ch into HMP showed very small particles together with aggregates of small particles probably formed during drying (Figure 9A). The same picture at higher magnification showed particles with a blurred contour and a mean size

of 50–70 nm (Figure 9B). The burred feature of particles did not come from a deficient focus, the particles had an actual diffuse surface upon drying because they were extensively swollen by water in their aqueous suspension. Denser particles with sharper edges and size of the order of 100 nm were observed in other parts of the grid (Figure 9C and D). Two different types of particles were coexisting, which indicated two different precipitation phenomena occurring during the precipitation process. Indeed, precipitation took place very fast as the addition of the Ch solution into the HMP solution was beginning because the concentration of HMP was high. Conversely, precipitation was slower at the end of mixing into the HMP solution that had a lower concentration because part of the HMP has precipitated. It is not possible to cause the formation of particles with a narrow size distribution when precipitation and mixing operate at the same rate. The mean size inferred from TEM was significantly smaller than measured by DLS (120 nm), confirming that the particles were swollen with water. The ratio of those mean sizes allowed an estimate of the swelling ratio (volume fraction of water inside particles) as

$$\phi_V(\text{water}) = 1 - \left[\frac{\text{Diam}(\text{TEM})}{\text{Diam}(\text{DLS})} \right]^3 \approx 0.7 \pm 0.2$$

The same type of observations were made for particles precipitated by pouring Ch into PP (Figure 9E and F). Pictures of particles precipitated by pouring HMP (or PP) into Ch showed very large particles coexisting with rather small ones. TEM did not allow imaging the largest ones. Figure 9G and H shows the smallest particles that were dense and spherical.

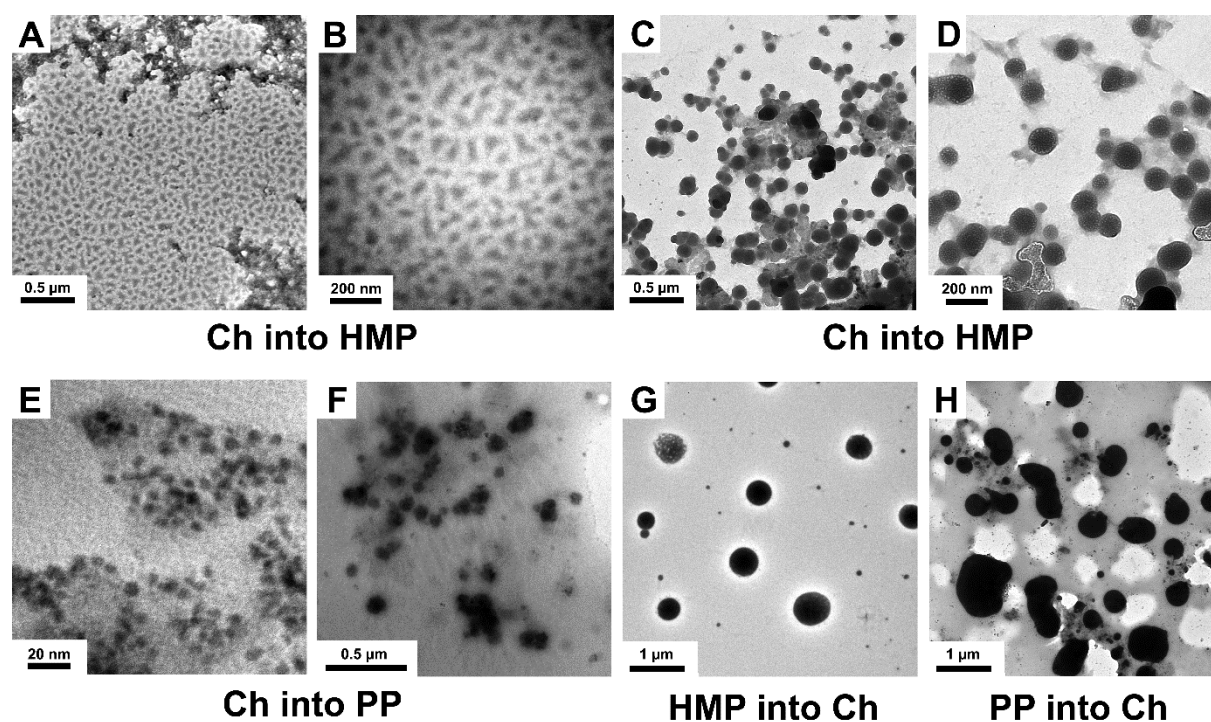


Figure 9. TEM pictures of particles precipitated by pouring Ch into HMP (A–D), Ch into PP (E, F), HMP into CH (G), and PP into Ch (H). See the text for more detailed descriptions.

Finally, the sodium salt of phytic acid allowed charge reversal because of its high negative charge (−6); but the particles were of very large size. Charge reversal required an excess of PA with respect to the charge stoichiometry, which meant that part of PA remained in solution in the aqueous phase. The presence of such hexavalent anions in the aqueous phase has a detrimental effect on the colloidal stability of particles. Thus, nanoparticles of Ch/PA possibly

formed by complex coacervation; but they aggregated into large particles because of their poor colloidal stability. Indeed, it is known from the DLVO theory that multivalent counterions efficiently cause the destabilization of colloidal suspensions. The Schulze–Hardy rule teaches that the colloidal stability decreases at the 6th power of the counterion valence [36]. As $6^6 = 4.7 \times 10^4$, the presence of residual PA in the aqueous phase had a huge effect on colloidal stability, even though its concentration might be low.

3.3. Encapsulation of the BSA protein

The two systems where charge inversion into negative was successful (Ch into HMP or PP) were selected for the encapsulation of BSA taken as a model case. The isoelectric point of BSA is at pH 4.7–5.0 [37,38], so that BSA is in its cationic form at pH 4. BSA is a globular protein at pH 4; its expansion in acidic medium occurs below pH 3.5 [39,40]. The particles obtained by pouring the Ch into HMP or PP solution showed a diameter and zeta potential of 123 nm and -21.5 mV or 162 nm and -29 mV, respectively. These nanoparticles loaded with BSA maintained the same size and ζ potential as their blank counterpart. This meant that the BSA charge was compensated by part of the HMP or PP. The amount of BSA was 1 mg against 5 mg of chitosan in 5 mL of water, which was approximately equivalent to increasing the chitosan concentration by 20%. Such small variation of the overall concentration of cationic species did not change the characteristics of the particles. The encapsulation efficiency was evaluated by measurements of BSA contents in the aqueous phase and inside the nanoparticles. 0.5 % of BSA was found in the supernatant of the Ch/HMP nanoparticles, while 85.7 % of BSA was recovered in the precipitate. For Ch/PP nanoparticles, the partition of BSA was 2.5 % in the aqueous phase and 92.9 % in the precipitate. The present encapsulation efficiency was much higher than reported in the literature for positively charged chitosan particles. As an example, Rampino *et al.* reported an *EE* in the range 40–60% for the Ch/TPP particles [24]. The same authors reported a variation of the zeta potential because they added BSA to a suspension of blank particles (after their preparation), whereas BSA was added together with Ch and co-precipitated by HMP or PP in the present case. The control of the pH over the whole preparation process is an absolute requirement for the encapsulation of fragile biomolecules such as proteins. The present process allows maintaining a constant pH value of 4 over the whole process while inverting the charge of chitosan. Complex encapsulation processes involving several steps at various pH are risky regarding the retention of the biological activity of the active substance. As an example, Gomathi *et al.* could successfully prepare blank Ch/PP and Ch/HMP particles of nanometric size [41]. However, their process started in a 2% aqueous acetic acid solution that the pH is 2.6, the mixture was centrifuged, dried and finally reconstituted in PBS. Neither the pH was controlled, nor the zeta potential was measured, so that it is not known whether the charge of chitosan has been reversed during precipitation. Encapsulation requires that the active substance is present at the precipitation step where it is co-precipitated, so that the starting pH should be kept high enough for avoiding degradation of the active substance in acidic medium. Though the final pH of the reconstituted dosage form is that of PBS, the process reported by Gomathi *et al.* is only useful for active substances that can sustain acidic media.

4. Conclusions

Hydrogel nanoparticles of negatively charged chitosan/hexametaphosphate (Ch/HMP) and chitosan/polyphosphate (Ch/PP) complex coacervate were prepared at pH 4 by simply mixing the aqueous solutions of the two partners. Such a mild preparation method allowed an efficient encapsulation of BSA, a positively charged protein used as a model active substance.

The manufacture of negatively charged particles required the charge reversal of chitosan by binding an excess negative charge coming from polyphosphates. Such charge reversal could be achieved by using highly charged HMP (charge -5 at pH 4) or PP, and switching the order of mixing from the usual addition of polyphosphate solution into the chitosan solution to the inverse order. Up to now, charge reversal could not be achieved because most studies were restricted to the use of tripolyphosphate (TPP) of charge -3 and only the order of mixing polyphosphate into chitosan was considered. Indeed, most studies reported in the literature so far refer to TPP used as a "cross-linking agent", which means that a small amount of TPP was added with respect to the charge stoichiometry and TPP was added into chitosan. This process was called "ionotropic gelation", suggesting that the amount of added cross-linking agent was restricted to that required to cause gelation. "Complex coacervation" would be a better terminology for the present process.

The mixing order of the solutions in the complex coacervation technique significantly changes the course of precipitation, making it possible to obtain nano- or microparticles of either negative or positive charge at pH 4 where chitosan is soluble in water.

Charge inversion of chitosan allows the encapsulation of positively charged proteins with an improved encapsulation efficiency ($\sim 90\%$) than in the usual TPP-based coacervate (less than 60% in the literature). The encapsulation of the bovine serum albumin at pH 4 is given as a case study of a positively charged protein.

Acknowledgments

This study was supported by a grant from the Coordenação de Aperfeiçoamento de Pessoal de Nível Superior - Brasil (CAPES) - Finance Code 001. We are grateful to Agnès Crepet (IMP, University of Lyon 1) who did SEC analyses of chitosan.

Declarations of interest: None

References

- [1] Desai K.G.H. Chitosan nanoparticles prepared by ionotropic gelation: An overview of recent advances, *Crit. Rev. Ther. Drug Carrier Systems* 33 (2016) 107–158.
- [2] Situ W., Xiang T., Liang Y. Chitosan-based particles for protection of proteins during storage and oral administration, *Int. J. Biol. Macromol.* 117 (2018) 308–314.
- [3] Sang Z., Qian J., Han J., Deng X., Shen J., Li G., Xie Y. Comparison of three water-soluble polyphosphate tripolyphosphate, phytic acid, and sodium hexametaphosphate as crosslinking agents in chitosan nanoparticle formulation, *Carbohydr. Polym.* 230 (2020) 115577.
- [4] Carvalho F.G., Magalhães T.C., Teixeira N.M., Gondim B.L.C., Carlo H.L., Santos R.L., Oliveira A.R., Denadai Â.M.L. Synthesis and characterization of TPP/chitosan nanoparticles: Colloidal mechanism of reaction and antifungal effect on *C. albicans* biofilm formation, *Mater. Sci. Eng. C*, 104 (2019) 109885.
- [5] Çakır M.A., İcyer N.C., Tornuk F. Optimization of production parameters for fabrication of thymol-loaded chitosan nanoparticles, *Int. J. Biol. Macromol.* 151 (2020) 230–238.

- [6] Kiaie N., Aghdam R.M., Tafti S.H.A., Emami S.H. Statistical optimization of chitosan nanoparticles as protein vehicles, using response surface methodology, *J. Appl. Biomater. Funct. Mater.* 14 (2016) e413–e422.
- [7] Anter H.M., Abu Hashim I.I., Awadin W., Meshali M.M. Novel chitosan oligosaccharide-based nanoparticles for gastric mucosal administration of the phytochemical “apocynin”, *Int. J. Nanomedicine* 14 (2019) 4911–4929.
- [8] Pant A., Negi J.S. Novel controlled ionic gelation strategy for chitosan nanoparticles preparation using TPP- β -CD inclusion complex, *Eur. J. Pharm. Sci.* 112 (2018) 180–185.
- [9] Shah B.R., Zhang C., Li Y., Li B. Bioaccessibility and antioxidant activity of curcumin after encapsulated by nano and Pickering emulsion based on chitosan-tripolyphosphate nanoparticles, *Food Res. Int.* 89 (2016) 399–407.
- [10] Li R., Wu Z., Wang Y., Ding L., Wang Y. Role of pH-induced structural change in protein aggregation in foam fractionation of bovine serum albumin, *Biotechnol. Rep.* 9 (2016) 46–52.
- [11] Wu Y., Wu J., Cao J., Zhang Y., Xu Z., Qin X., Wang W., Yuan Z. Facile fabrication of poly(acrylic acid) coated chitosan nanoparticles with improved stability in biological environments, *Eur. J. Pharm. Biopharm.* 112 (2017) 148–154.
- [12] Jaiswal S., Dutta P.K., Kumar S., Koh J., Pandey S. Methyl methacrylate modified chitosan: Synthesis, characterization and application in drug and gene delivery, *Carbohydr. Polym.* 211 (2019) 109–117.
- [13] Chen K.-Y., Zeng S.-Y. Fabrication of quaternized chitosan nanoparticles using tripolyphosphate/genipin dual cross-linkers as a protein delivery system, *Polymers* 10 (2018) 1226.
- [14] Hosseini S.F., Soleimani M.R., Nikkhah M. Chitosan/sodium tripolyphosphate nanoparticles as efficient vehicles for antioxidant peptidic fraction from common kilka, *Int. J. Biol. Macromol.* 111 (2018) 730–737.
- [15] Du Z., Liu J., Zhang T., Yu Y., Zhang Y., Zhai J., Huang H., Wei S., Ding L., Liu B. A study on the preparation of chitosan-tripolyphosphate nanoparticles and its encapsulation mechanism for egg white derived peptides, *Food Chem.* 286 (2019) 530–536.
- [16] Stie M.B., Thoke H.S., Issinger O.-G., Hochscherf J., Guerra B., Olsen L.F. Delivery of proteins encapsulated in chitosan-tripolyphosphate nanoparticles to human skin melanoma cells, *Colloids Surfaces B: Biointerfaces* 174 (2019) 216–223.
- [17] Raja M.A.G., Katas H., Wen T.J. Stability, intracellular delivery, and release of siRNA from chitosan nanoparticles using different cross-linkers, *PLoS ONE* 10 (2015) e0128963.
- [18] Calvo P., Remuñan-López C., Vila-Jato J.L., Alonso M.J. Novel hydrophilic chitosan–polyethylene oxide nanoparticles as protein carriers, *J. Appl. Polym. Sci.* 63 (1997) 125–132.
- [19] Calvo P., Remuñan-López C., Vila-Jato J.L., Alonso M.J. Chitosan and chitosan/ethylene oxide-propylene oxide block copolymer nanoparticles as novel carriers for proteins and vaccines, *Pharm. Res.* 14 (1997) 1431–1436.
- [20] Bugnicourt L., Ladavière C. Interests of chitosan nanoparticles ionically cross-linked with tripolyphosphate for biomedical applications, *Progr. Polym. Sci.* 60 (2016) 1–17.
- [21] Dudhani A.R., Kosaraju S.L. Bioadhesive chitosan nanoparticles: Preparation and characterization, *Carbohydr. Polym.* 81 (2010) 243–251.
- [22] Rodrigues S., Costa A.M.R., Grenha A. Chitosan/carrageenan nanoparticles: Effect of cross-linking with tripolyphosphate and charge ratios, *Carbohydr. Polym.* 89 (2012) 282–289.
- [23] Fàbregas A., Miñarro M., García-Montoya E., Pérez-Lozano P., Carrillo C., Sarrate R., Sánchez N., Ticó J.R., Suñé-Negre J.M. Impact of physical parameters on particle size and reaction yield when using the ionic gelation method to obtain cationic polymeric chitosan–tripolyphosphate nanoparticles, *Int. J. Pharm.* 446 (2013) 199–204.
- [24] Rampino A., Borgogna M., Blasi P., Bellich B., Cesàro A. Chitosan nanoparticles: Preparation, size evolution and stability, *Int. J. Pharm.* 455 (2013) 219–228.

- [25] Silva N.C., Silva S., Sarmiento B., Pintado M. Chitosan nanoparticles for daptomycin delivery in ocular treatment of bacterial endophthalmitis, *Drug Delivery* 22 (2015) 885–893.
- [26] Rázga F., Vnuková D., Némethová V., Mazancová P., Lacík I. Preparation of chitosan-TPP sub-micron particles: Critical evaluation and derived recommendations, *Carbohydr. Polym.* 151 (2016) 488–499.
- [27] Hejjaji E.M.A., Smith A.M., Morris G.A. Designing chitosan-tripolyphosphate microparticles with desired size for specific pharmaceutical or forensic applications, *Int. J. Biol. Macromol.* 95 (2017) 564–573.
- [28] Bangun H., Tandiono S., Arianto A. Preparation and evaluation of chitosan-tripolyphosphate nanoparticles suspension as an antibacterial agent, *J. Appl. Pharm. Sci.* 8 (2018) 147–156.
- [29] Hirai A., Odani H., Nakajima A. Determination of degree of deacetylation of chitosan by ¹H NMR spectroscopy, *Polym. Bull.* 26 (1991) 87–94.
- [30] Vårum K.M., Anthonsen M.W., Grasdalen H., Smidsrød O. Determination of the degree of *N*-acetylation and the distribution of *N*-acetyl groups in partially *N*-deacetylated chitins (chitosans) by high-field n.m.r. spectroscopy, *Carbohydr. Res.* 211 (1991) 17–23.
- [31] Lavertu M., Xia Z., Serreqi A.N., Berrada M., Rodrigues A., Wang D., Buschmann M.D., Gupta A. A validated ¹H NMR method for the determination of the degree of deacetylation of chitosan, *J. Pharm. Biomed. Anal.* 32 (2003) 1149–1158.
- [32] Rashidipour M., Maleki A., Kordi S., Birjandi M., Pajouhi N., Mohammadi E., Heydari R., Rezaee R., Rasoulilian B., Davari B. Pectin/chitosan/tripolyphosphate nanoparticles: Efficient carriers for reducing soil sorption, cytotoxicity, and mutagenicity of paraquat and enhancing its herbicide activity, *J. Agric. Food Chem.* 67 (2019) 5736–5745.
- [33] Bagre A.P., Jain K., Jain N.K. Alginate coated chitosan core shell nanoparticles for oral delivery of enoxaparin: *In vitro* and *in vivo* assessment, *Int. J. Pharm.* 456 (2013) 31–40.
- [34] Motiei M., Sedlářik V., Lucia L.A., Fei H., Munster L. Stabilization of chitosan-based polyelectrolyte nanoparticle cargo delivery biomaterials by a multiple ionic cross-linking strategy, *Carbohydr. Polym.* 231 (2020) 115709.
- [35] Rinaudo M., Pavlov G., Desbrières J. Influence of acetic acid concentration on the solubilization of chitosan, *Polymer* 40 (1999) 7029–7032.
- [36] Hiemenz P.J., Rajapopalan R. *Principles of Colloid and Surface Chemistry*. 3rd ed, Marcel Dekker, New York, (1997) 588–591.
- [37] Longsworth L.G., Jacobsen C.F. An electrophoretic study of the binding of salt ions by β -lactoglobulin and bovine serum albumin, *J. Phys. Colloid Chem.* 53 (1949) 126–135.
- [38] Meechai N., Jamieson A.M., Blackwell J. Translational diffusion coefficients of bovine serum albumin in aqueous solution at high ionic strength, *J. Colloid Interface Sci.* 218 (1999) 167–175.
- [39] Yang J.T., Foster J.F. Changes in the intrinsic viscosity and optical rotation of bovine plasma albumin associated with acid binding, *J. Am. Chem. Soc.* 76 (1954) 1588–1595.
- [40] Sogami M., Foster J.F. Isomerization reactions of charcoal-defatted bovine plasma albumin. The N–F transition and acid expansion. *Biochemistry* 7 (1968) 2172–2182.
- [41] Gomathi T., Prasad P.S., Sudha P.N., Anil S. Size optimization and *in vitro* biocompatibility studies of chitosan nanoparticles, *Int. J. Biol. Macromol.* 104 (2017) 1794–1806.

SUPPLEMENTARY MATERIAL

Negatively charged chitosan nanoparticles by ionotropic gelation for encapsulation of positively charged proteins

Melissa Marques Gonçalves^{a,b}, Daniela Florencio Maluf^b, Roberto Pontarolo^b, Cyro Ketzer Saul^b, Eyad Almouazen^a, Yves Chevalier^a,

^a *Laboratory of Automatic Control, Chemical and Pharmaceutical Engineering (LAGEPP), University Claude Bernard Lyon 1, 69622 Villeurbanne, France.*

^b *Federal University of Paraná (UFPR), 80210-170, Curitiba, Brazil.*

1. Characterization of Chitosan

1.1. Degree of acetylation

The ¹H NMR spectrum of chitosan was recorded with a Bruker AV400 spectrometer in solution into D₂O/DCI (2 mg chitosan and 20 μL DCI 10 M in 1 mL D₂O) solution at 70 °C according to [1–3]. Heating at 70 °C was necessary for shifting the line of HDO upfield to lower than 4.5 ppm such that the line of H1 protons correctly appeared at 4.91 ppm. The degree of acetylation of chitosan was determined from the integrals of the N-acetyl line at 2.07 ppm with respect to that of protons H1 (4.91 ppm), H2 (3.23 ppm) and H3-6 (3.5–4.1 ppm). The acetylation degree was $DA = 20\%$. Accordingly, the molar mass of the mean repeat unit is:

$$M_{\text{mol}} = DA \times M_{\text{mol}}(\text{acetylglucosamine}) + (1 - DA) \times M_{\text{mol}}(\text{glucosamine}),$$

$$M_{\text{mol}} = 0.2 \times 203.19 + 0.8 \times 161.16 = 169.57 \text{ g} \cdot \text{mol}^{-1}.$$

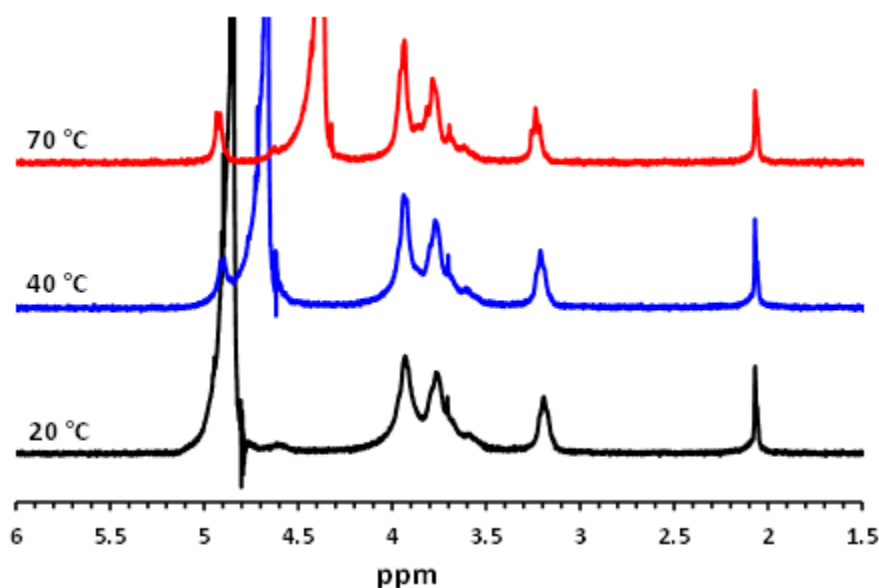


Figure S1. ¹H NMR spectra of chitosan in D₂O/DCI solution at 20, 40 and 70 °C.

1.2. Molar mass

The molar mass of chitosan was determined by SEC analysis in acetate buffer pH 4.8 using a Wyatt instrument equipped with TSK6000 and TSK2500 columns and with refractive index, multi-angle light scattering (MALS) and dynamic light scattering detectors (Figure S2). The refractive index detection allowed the determination of the specific refractive index increment $dn/dC = 0.1840 \text{ mL} \cdot \text{g}^{-1}$. The number-average and mass-average molar masses of chitosan were

determined from the Zimm plot of MALS as $M_N = 9.95 \cdot 10^4 \text{ g}\cdot\text{mol}^{-1}$ and $M_W = 2.60 \cdot 10^5 \text{ g}\cdot\text{mol}^{-1}$ (polydispersity index $M_W/M_N = 2.6$).

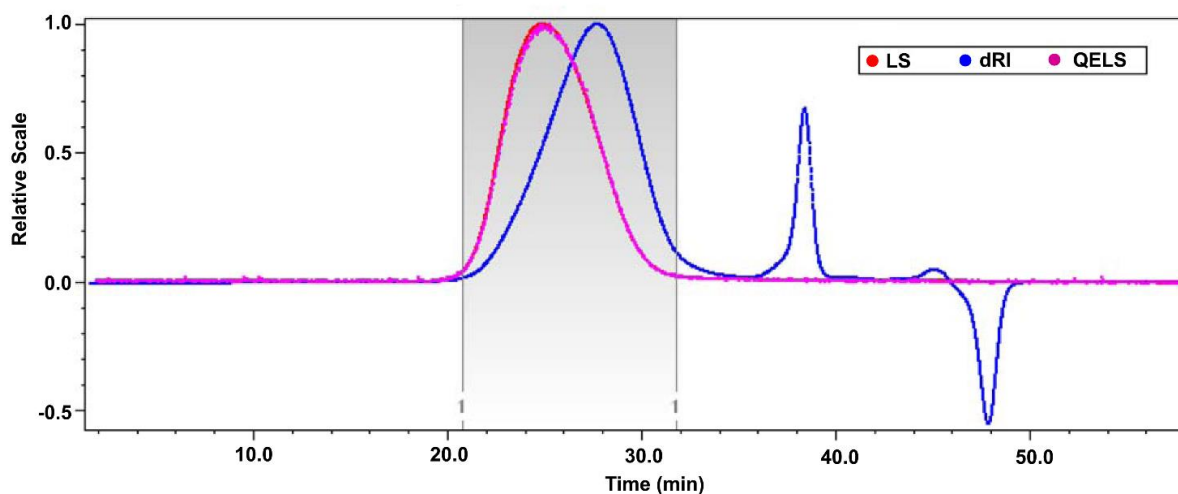


Figure S2. Traces of the detectors of the SEC analysis of chitosan (LS = Light Scattering, dRI = differential Refractive Index, QELS = Quasi-Elastic Light Scattering or Dynamic Light Scattering).

2. Characterization and electrical charge of polyphosphates

2.1. Chemical analysis

The six studied polyphosphates are characterized by their different numbers of phosphate groups: $n = 1$ for orthophosphate, $n = 2$ for pyrophosphate, $n = 3$ for tripolyphosphate, $n = 6$ for hexametaphosphate and phytate, and $n > 6$ for polyphosphate. Some of them are not pure compounds however. ^{31}P NMR spectra of polyphosphates solutions in D_2O were collected using a Bruker AV400 spectrometer under broadband proton decoupling. Chemical shifts were referred to H_3PO_4 85 %. The spectra of orthophosphate and pyrophosphate showed a single peak in agreement with expectations for pure compounds (Figure S3). Tripolyphosphate, that actually is the linear triphosphate, showed two peaks corresponding to the expected central (a triplet at -21.92 ppm , $^2J_{\text{POP}} = 21 \text{ Hz}$) and external (a doublet at -7.96 ppm , $^2J_{\text{POP}} = 21 \text{ Hz}$) phosphate groups; and it contained a small fraction (5 mol%) of orthophosphate as revealed by a peak at 1.32 ppm .

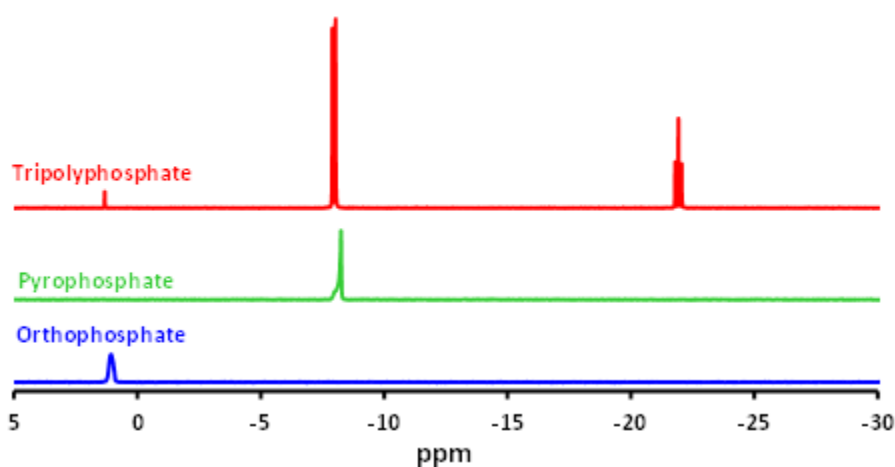


Figure S3. ^{31}P NMR spectra of orthophosphate, pyrophosphate and tripolyphosphate.

The spectra of hexametaphosphate and polyphosphate were rather similar (Figure S4). The expected spectrum of hexametaphosphate should show a single peak because all phosphorus atoms are equivalent in the cyclic structure of hexametaphosphate. Indeed, the spectrum showed an intense resonance at -21.7 ppm. A supplementary peak at -8.25 ppm indicated the presence of pyrophosphate accounting for 20 % of the phosphorus content. The spectrum of polyphosphate is similar because the resonances of both cyclic and linear polyphosphates with $n > 5$ appear between -20.5 ppm and -23.0 ppm. Linear polyphosphates can be distinguished by the peak of the chain ends at -10 ppm. Indeed, the spectrum of polyphosphate showed such a latter characteristic peak. The polyphosphate may contain a few cyclic polyphosphates together with the main mixed linear polyphosphates. It also contains a small amount of orthophosphate. The spectrum of hexametaphosphate also showed a small peak at -10 ppm that indicated the presence of a small part of linear polyphosphate together with the main cyclic hexametaphosphate.

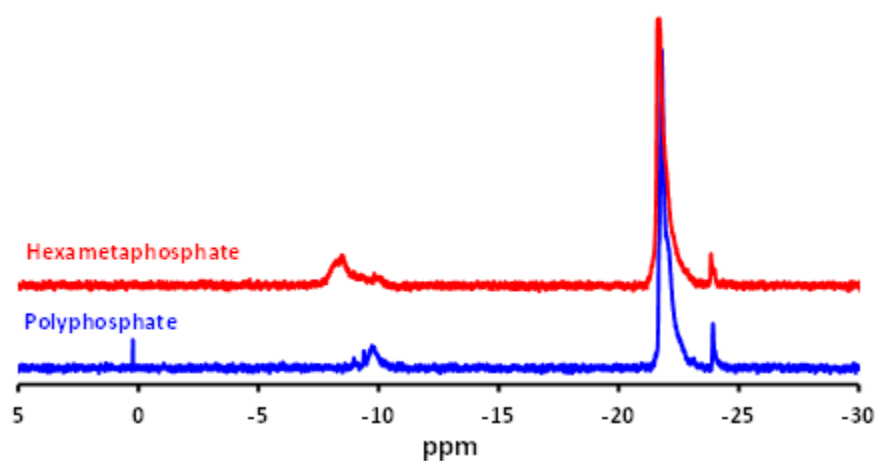


Figure S4. ^{31}P NMR spectra of hexametaphosphate and polyphosphate.

All polyphosphates, as delivered by the supplier, were partly under their sodium salt form. Their degree of neutralization was not specified. Elemental analysis of sodium and phosphorus in solutions of polyphosphates at 1000, 2000, 3000 and 5000 ppm concentration were performed by MP-AES with a Agilent 4200 MP-AES instrument. Calibration was done with solutions of disodium hydrogen orthophosphate in 1 M HCl solution. Samples were hydrolyzed in 1 M HCl solution at $50\text{ }^{\circ}\text{C}$ for 24 h in order to convert polyphosphates into the same orthophosphate species as for the calibration. Detection used the strong emission lines of sodium at 330.327 nm and 568.820 nm and those of phosphorus at 213.618 nm, 214.915 nm and 253.560 nm. According to these analyses, the pyrophosphate, tripolyphosphate and hexametaphosphate were indeed under their fully neutralized form $\text{Na}_4\text{P}_2\text{O}_7$, $\text{Na}_5\text{P}_3\text{O}_{10}$ and $\text{Na}_6\text{P}_6\text{O}_{18}$. The polyphosphate analysis corresponded to $\text{Na}_n\text{H}_2\text{P}_n\text{O}_{3n+1}$ instead of $\text{Na}_{n+2}\text{P}_n\text{O}_{3n+1}$ for the fully neutralized form of linear polyphosphate. This meant that the two phosphate groups at chain ends were under their OPO_3HNa form. Finally, phytate was under the form $\text{Na}_6\text{C}_6\text{H}_{12}\text{P}_6\text{O}_{24}$ or $(\text{CHOPO}_3\text{HNa})_6$, which corresponded to half neutralization of all phosphate monoester groups.

2.2. Electrical charge at pH 4

The pH was set at 4 in all experiments by addition of acetic acid. This was required for ensuring that chitosan is soluble in water. The electrical charge of polyphosphates at pH 4 might have

been calculated from their pK_A 's. Unfortunately, several pK_A values are not documented; the situation is especially difficult for polyphosphate that is a mixture of several oligomeric polyphosphates. Furthermore, published data taken from different sources appear contradictory. As example, several fairly different sets of values have been reported for the 12 pK_A values of phytic acid (Table S1) [4–6].

The electrical charge of all compounds at pH 4 was determined from their chemical analysis and the volume of acid required to set pH = 4. The chemical analysis of supplied compounds by MP-AES taught their degree of neutralization, and the volume of HCl 1 M required to shift the pH down to 4 gave the amount of charge removal by acidification. Electrical charges were also calculated from the pK_A 's in cases where full sets of values were available.

Table S1. List of the studied polyphosphates together with their number of phosphorus atoms, pK_A 's and their negative electrical charge at pH 4.

Type of sodium polyphosphate	Number of phosphorus atoms	pK_A 's	ref	Charge at pH 4	
				calculated	inferred from titration
Orthophosphate	$n = 1$	2.148; 7.198; 12.319	[7]	-0.99	-0.97
Pyrophosphate	$n = 2$	0.91; 2.10; 6.70; 9.32	[8]	-1.99	-1.94
Triphosphate	$n = 3$	0; 1.1; 2.3; 6.3; 8.9	[9]	-2.98	-3.03
Hexametaphosphate	$n = 6$	–		–	-5.0
Polyphosphate	$n \approx 6$	–		–	-5.0
Phytate	$n = 6$	1.1; 1.5 ($\times 2$); 1.7; 2.1 ($\times 2$); 5.70; 6.85; 7.60; 10.0 ($\times 2$); 12.0	[4]	-6.01	-6.04
		1.59 ($\times 5$); 2.62; 4.86; 6.33; 8.28; 9.75 ($\times 3$)	[6]	-6.09	-6.04

3. Calibration of the Bradford method for analysis of BSA

The calibration curve of absorbance at 595 nm wavelength (Abs) was determined for BSA concentrations up to $16 \text{ mg}\cdot\text{L}^{-1}$. Data points were regressed to a 3rd degree polynomial as $C (\text{mg}\cdot\text{L}^{-1}) = 106.5 Abs^3 - 16.2 Abs^2 + 6.9 Abs + 0.1$ (Figure S5).

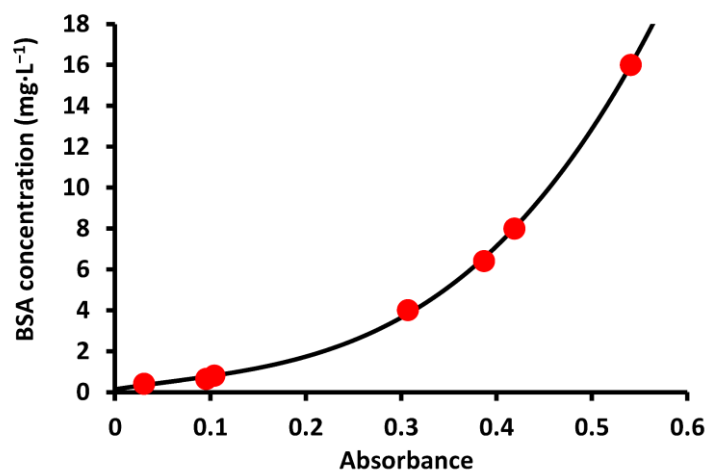


Figure S5. Calibration curve for the Bradford assay analysis of BSA by the absorbance at 595 nm.

4. Degradation of coacervate particles under the electron beam of TEM

All coacervate samples underwent degradation in the electron microscope. This was clearly observed with the densest particles by the appearance and growth of white holes that were bubbles of degradation products inside particles. This was quite a fast phenomenon occurring within a few minutes once the electron beam was focusing on the samples. The growth of gas bubbles inside particles deformed them and caused coalescence of particles that were at close contact. Most of the particles were at close contact on the TEM grid as a consequence of drying the aqueous suspension before TEM observation. That particles appeared aggregated on the TEM grid did not indicate any aggregation occurring in the aqueous suspension. Aggregation was the consequence of drying the samples. Bubbles disappear after a while because the electron microscope works under vacuum, and the holes heal back to recover the initial internal density of the particles.

A typical sequence of particles degradation under the electron beam is shown in [Figure S6](#). This compromised a correct tuning of the focus. Thus, focusing was done as fast as possible for degradation did not significantly change the morphology of the particles. Alternatively, once a precise focusing has been reached on particles undergoing degradation, the electron beam was shifted to another part of the sample for a very fast picture of fresh particles could be taken.

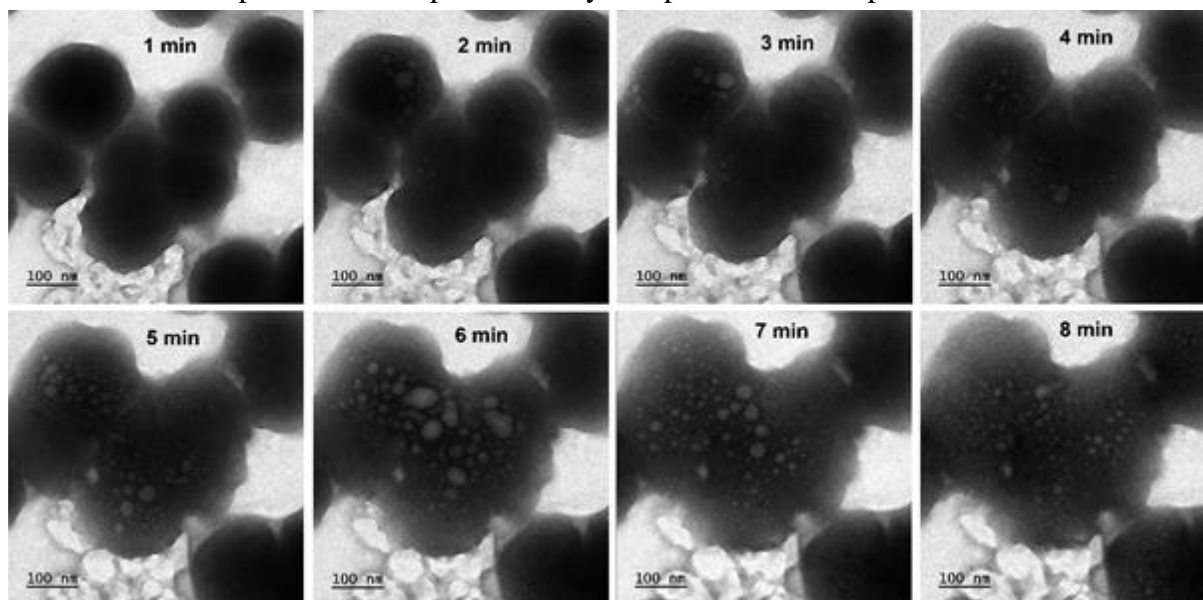


Figure S6. TEM pictures of Ch-HMP particles taken at different times under the electron beam. The sample was prepared by pouring 50 mL of 1 g·L⁻¹ Ch solution into 20 mL of 5 g·L⁻¹ HMP solution, and then diluting the suspension of particles to 1/100 with water. The successive pictures show particles at close contact where white gas bubbles of degradation products arose and expanded the particles to such a way that they merged into larger particles by coalescence.

References

- [1] Hirai A., Odani H., Nakajima A. Determination of degree of deacetylation of chitosan by ¹H NMR spectroscopy. *Polym. Bull.* 26 (1991) 87–94, doi:[10.1007/BF00299352](https://doi.org/10.1007/BF00299352).
- [2] Vårum K.M., Anthonsen M.W., Grasdalen H., Smidsrød O. Determination of the degree of *N*-acetylation and the distribution of *N*-acetyl groups in partially *N*-deacetylated chitins (chitosans) by high-field n.m.r. spectroscopy. *Carbohydr. Res.* 211 (1991) 17–23, doi:[10.1016/0008-6215\(91\)84142-2](https://doi.org/10.1016/0008-6215(91)84142-2).
- [3] Lavertu M., Xia Z., Serreqi A.N., Berrada M., Rodrigues A., Wang D., Buschmann M.D., Gupta A. A validated ¹H NMR method for the determination of the degree of deacetylation of chitosan. *J. Pharm. Biomed. Anal.* 32 (2003) 1149–1158, doi:[10.1016/S0731-7085\(03\)00155-9](https://doi.org/10.1016/S0731-7085(03)00155-9).
- [4] Costello A.J.R., Glonek T., Myers T.C. ³¹P nuclear magnetic resonance – pH titrations of *myo*-inositol hexaphosphate. *Carbohydr. Res.* 46 (1976) 159–171, doi:[10.1016/S0008-6215\(00\)84287-1](https://doi.org/10.1016/S0008-6215(00)84287-1).

- [5] Emsley J., Niazi S. The structure of *myo*-inositol hexaphosphate in solution: ³¹P N.M.R. investigation. *Phosphorus Sulfur* 10 (1981) 401–408, doi:[10.1080/03086648108077394](https://doi.org/10.1080/03086648108077394).
- [6] Martin C.J., Evans W.J. Phytic acid-metal ion interactions. II. The effect of pH on Ca(II) binding. *J. Inorg. Biochem.* 27 (1986) 17–30, doi:[10.1016/0162-0134\(86\)80105-2](https://doi.org/10.1016/0162-0134(86)80105-2).
- [7] Westheimer F.H. Why nature chose phosphates. *Science* 235 (1987) 1173–1178, doi:[10.1126/science.2434996](https://doi.org/10.1126/science.2434996).
- [8] Mitra R.P., Malhotra H.C., Jain D.V.S. Dissociation equilibria in pyrophosphates and kinetics of degradation. Part 1. – Dissociation constants of pyrophosphoric acid. *Trans. Faraday Soc.* 62 (1966) 167–172, doi:[10.1039/TF9666200167](https://doi.org/10.1039/TF9666200167).
- [9] Rasković P. Step-by-step process integration method for the improvements and optimization of sodium tripolyphosphate process plant. *Energy* 32 (2007) 983–998, doi:[10.1016/j.energy.2006.10.004](https://doi.org/10.1016/j.energy.2006.10.004).